ISIJ International, Vol. 51 (2011), No. 3, pp. 448–455

Characterisation of PVD-TiN Coated Austempered Ductile Iron: Effects of Nodule Count and Austempering Temperature

Diego A. COLOMBO,[1,2] María D. ECHEVERRÍA,[1] Osvaldo J. MONCADA[1,2] and Juan M. MASSONE[2]

1) Mechanical Technology Group, School of Engineering-Universidad Nacional de Mar del Plata, 4302 J.B. Justo Av., (B7608FDQ) Mar del Plata, Argentina. E-mail: diegocolombo@fi.mdp.edu.ar 2) Metallurgy Division, INTEMA-CONICET, School of Engineering-Universidad Nacional de Mar del Plata, 4302 J.B. Justo Av., (B7608FDQ) Mar del Plata, Argentina.

(*Received on July 20, 2010; accepted on December 2, 2010*)

In this work PVD-TiN coatings are deposited on ADI substrates austempered at 280 and 360°C, with nodule counts varying between 490 and 1 100 nod/mm^2. The deposition is performed at 300°C by the arc ion plating technique. The effects of the substrates' microstructure on the characteristics of the coatings and the possible changes in ausferritic microstructure owing to the effects of the deposition process are evaluated. The existing phases, preferred orientation, film thickness, hardness, Young's modulus, surface topography and adhesion of each coated sample are determined. A metallographic characterisation of the ausferritic matrices and determination of the retained austenite content are performed before and after deposition.

The results obtained indicate that PVD-TiN coatings feature a preferred orientation of (111) planes parallel to the surface and film thicknesses of about 2 μm. Knoop hardness is influenced by the substrates characteristics, the values range from 1 700 to 2 100 $HK_{0.015}$. Nanohardness values are close to 25 GPa, while Young's modulus shows some scattering (323 to 336 GPa). The surface topography is dependent on the microstructure of the substrates and the surface preparation method employed as well as on the deposition process used. The adhesion strength quality of the coatings, according to the Rockwell-C adhesion test, can be related to HF1–HF2 and is affected neither by the hardness differences between the different substrates nor by the nodule count variation. After the coating process, the microstructure of ADI substrates only suffers negligible changes and the amount of retained austenite decreases slightly.

KEY WORDS: austempered ductile iron; physical vapour deposition; TiN coatings; adhesion.

1. Introduction

Austempered ductile iron (ADI), in its different grades (1 to 5 ASTM 897-90 standard), has opened new applications in the manufacturing of mechanical components[1,2] given the wide range of mechanical properties achievable after the proper adjustment of the chemical composition and heat treatment parameters, as well as its advantageous features, if compared with high-strength cast steels, such as its lower cost and weight, greater flexibility in parts design, similar fatigue performance and comparable tensile strength and wear resistance.[3]

The progress achieved in casting technology during the last decades has allowed the metalcasting industry to obtain castings with a wall thickness thinner than 5 mm.[4] Moreover, the greater cooling rate with respect to conventional thickness has led to a sharp increase of nodule count and to a microstructure refinement,[5] which has enhanced the mechanical properties.[6,7]

Ausferritic microstructure comprise a fine mixture of acicular ferrite and metastable austenite of high carbon content. Austenite is retained at room temperature because bainitic ferrite growth increases the local carbon content of the adjacent austenite, so decreasing martensite start temperature (Ms) to below room temperature. Provided sufficient temperature and time is given, austenite can lower its energy by transforming itself into a mixture of ferrite and cementite, thereby deteriorating the mechanical properties of the material.[8]

It is widely recognised that the tribological performance of engineering materials are strongly dependent on the properties and characteristics of their surface, mainly hardness, surface roughness, friction coefficient and residual stresses, all of them improvable by surface treatments. Notwithstanding this, any surface treatment involving ADI exposure to high temperature during long periods could activate the decomposition mechanisms of retained austenite previously described.

The deposition of thin-hard films by physical vapour deposition (PVD) is an effective means of optimising the mechanical properties of heat treated parts, due to its relatively low processing temperature (200 to 500°C) as compared to other surface treatments. Studies undertaken on ADI substrates of conventional nodule count and 360°C austempering temperature with coatings of different materials and monolayered or multilayered structures, have accounted for improvements in mechanical properties and corrosion resistance.[9–11] All studies applied processing

temperatures of up to 300°C; and reported no deterioration of ADI's microstructure.

Coating properties rely markedly on substrates characteristics (cleaning prior to deposition, microstructure, surface topography, mechanical properties, physicochemical compatibility with the coating material), on the PVD technique utilised and on the processing parameters (chamber pressure, angle of incidence and distribution of gas flow, current density, bias voltage, substrate temperature).[12)]

In this work PVD-TiN coatings are deposited on ADI substrates of different nodule count, austempered at 280 and 360°C. The coating process is performed applying the arc ion plating technique, using an industrial reactor and under process parameters specifically selected for this material. The effects of the substrates' microstructure on the characteristics of the coatings are studied and the possible changes in ausferritic microstructure owing to the effects of the coating process are evaluated.

2. Experimental Procedures

2.1. Substrate Material and Samples Preparation

The material utilised in this work was ductile iron produced in a 55 kg middle-frequency induction furnace (3 kHz), following conventional practices of melting, nodularising, inoculation and casting into sand moulds. The furnace was charged with pig iron (31%), steel scrap (65%); and the rest was recarburiser and ferrosilicon.

The charge was melted and superheated to 1 550°C. The liquid metal was extracted and treated in separate ladles using the two step method. Nodularising was carried out in the first ladle using a 1.40% of FeSiMg (6% Mg) and the sandwich method. Inoculation was performed during the transfer to the second ladle, by adding a 0.65% of FeSi (75% Si) to the stream.

The melt was poured into vertical moulds designed to yield 4 and 6 mm thick plates, and into Y-blocks of 13 mm, obtaining three different nodule counts. The chemical composition of the material (wt%), analysed by a Baird DV6 optical emission spectrometer, was as follows: C: 3.4; Si: 2.7; Mn: 0.21; S: 0.008; P: 0.027; Mg: 0.033 and Fe balanced. CE: 4.3.

The plates and Y-blocks were cut and machined in order to obtain prismatic samples of nominal dimensions 25×25×3.5 mm approximately.

The samples were divided into two groups, and each group was subjected to different austempering heat treatment. The heat treatments consisted in austenitising at 910°C for 120 min, austempering in a salt bath at temperatures of 280 and 360°C for 90 min, and subsequent air cooling to room temperature.

Finally, all treated samples were subjected to a progressive manual polishing with SiC waterproof paper up to 1 000 grit size.

The samples austempered at 280 and 360°C were identified as ADI280 and ADI360, respectively.

2.2. PVD Coating Process

TiN coatings were obtained applying the arc ion plating (AIP) technique, using an industrial reactor. Prior to this, the samples had been thoroughly degreased, ultrasonically cleaned, rinsed with alcohol and dried with warm air. Inside the chamber, and prior to deposition, samples were cleaned once again by bombardments with energetic titanium ions, thereby eliminating oxides debris and other contaminants. **Table 1** lists the processing parameters.

2.3. Substrates and Coatings Characterisation

The values of nodule count average corresponding to each cast thickness were determined by optical microscopy (Olympus PMG3) and digital image processing, taking a nodule diameter of 5 μm as threshold value. Vickers hardness (30 kg load) of the treated samples was established using a Durotest DU250 universal hardness tester. **Table 2** lists the nodule count and Vickers hardness values of the different substrates. According to comparisons with charts, the nodularity exceeded 90% in all the casting thicknesses.

X-Ray diffraction (XRD) was performed for phase identification in substrates and coatings. A Phillips PW 1830/00 diffractometer was utilised, with Co Kα radiation (λ= 1.7890 Å) at 40 kV and 30 mA. XRD patterns were recorded in a 2θ range from 30° to 65°, in steps of 0.01° and with a velocity of 1° min^{-1}.

In order to analyse the effects of the PVD coating process on the substrates' microstructure, a metallographic characterisation was conducted, and the amount of retained austenite and Knoop hardness of the ausferritic matrices were established before and after coating deposition. Optical microscopy was applied to perform the metallographic characterisation. XRD patterns of ADI substrates were employed to determine the amount of retained austenite, using the software PowderCell. The coatings were removed by manual polishing with SiC waterproof paper to record the XRD patterns of the substrates after deposition. The hardness of the treated samples was determined using a Leitz Wetzlar microhardness tester. All the measurements were performed using a 15 g load.

The effects of the PVD process on the surface topography of the samples were assessed by analysing two roughness parameters: the arithmetic average roughness (Ra) and the surface skewness (Rsk). The arithmetic average rough-

Table 1. Processing parameters of the AIP process.

Coating type	TiN
Target material	Ti (99.9%)
Substrate-target distance [mm]	200
Reactive gas	N_2
Substrate BIAS voltage [V]	-250
Arc current [A]	65
Chamber pressure [Pa]	2
Substrate temperature [°C]	300
Deposition time [min]	120

Table 2. Nodule count and Vickers hardness of the different substrates.

Sample	Casting thickness [mm]	Nodule count [nod/mm^2]	Hardness [HV_{30}]
ADI280	13 (Y–block)	494	454
	6 (plate)	593	481
	4 (plate)	1056	511
ADI360	13 (Y–block)	494	348
	6 (plate)	593	366
	4 (plate)	1056	385

ness is the average of the absolute values of the measured height deviations from the surface mean line. Surface skewness, in turn, represents the asymmetry of the surface profile from the surface mean line. This means that profiles with peaks removed or deep scratches yield negative skewness, whereas profiles with valleys filled in or high peaks yield positive skewness.[13] A profilometer (Taylor Hobson Surtronic 3+) was used to measure the roughness parameters of the samples before and after coating deposition within an evaluation length of 4 mm (cut-off, 0.8 mm). In addition, cross sectional views and the surface morphology of the coated samples were analysed using optical microscopy and SEM (JEOL JSM-6460LV).

Coatings thickness was measured on fractured cross sections micrographs, obtained by SEM.

The hardness of the coated samples was determined by performing Knoop microhardness tests, using a 15 g load.

Instrumented nanoindentation tests were conducted using a Hysitron TI 900 Triboindenter device equipped with a Berkovich diamond indenter. The indentations were performed under a load control mode, applying a 14 mN maximum load. The machine compliance and tip geometry were calibrated using the Oliver–Pharr method.[14] The hardness and reduced modulus of the coated samples were calculated with the device software, using the Oliver–Pharr method.[14]

Young's modulus of a coated sample can be obtained from reduced modulus data, applying the following expression:

$$\frac{1}{Er} = \frac{1-\nu_m^2}{E_m} + \frac{1-\nu_i^2}{E_i}$$

were the subscripts m and i are denoted as the coated sample and the indenter tip, respectively. E is the Young's modulus and ν is the Poisson's ratio. The indenter properties used in this study's calculations are E_i=1 140 GPa and ν_i= 0.07. A Poisson's ratio ν_m=0.25 was assumed for TiN.[15]

Coating adhesion was evaluated using the Rockwell-C adhesion test. A series of indentations were made using a 150 kg load. After indentation, an optical microscope with a magnification of 100 : 1 was used to observe the damage adjacent to the indentations boundary. The damage to the coatings was compared with an adhesion strength quality pattern defined from HF1 to HF6. HF1 to HF4 indices represent good adhesion, whereas HF5 and HF6 stand for insufficient adhesion.[16]

3. Results and Discussion

The results are shown in the following order: phases identified in substrates and coatings, microstructure of the substrates before and after coating process, surface topography of the samples before and after coating process and, finally, characteristics of film thickness, hardness, Young's modulus and adhesion of the coatings.

3.1. Phase Identification

Figures 1 and **2** illustrate the XRD patterns of the samples studied before and after coating deposition. The patterns of the uncoated samples depict the main diffraction peaks of ferrite phase (Fe-α) and austenite phase (Fe-γ), whose relative intensities are in accordance with the ausfer-

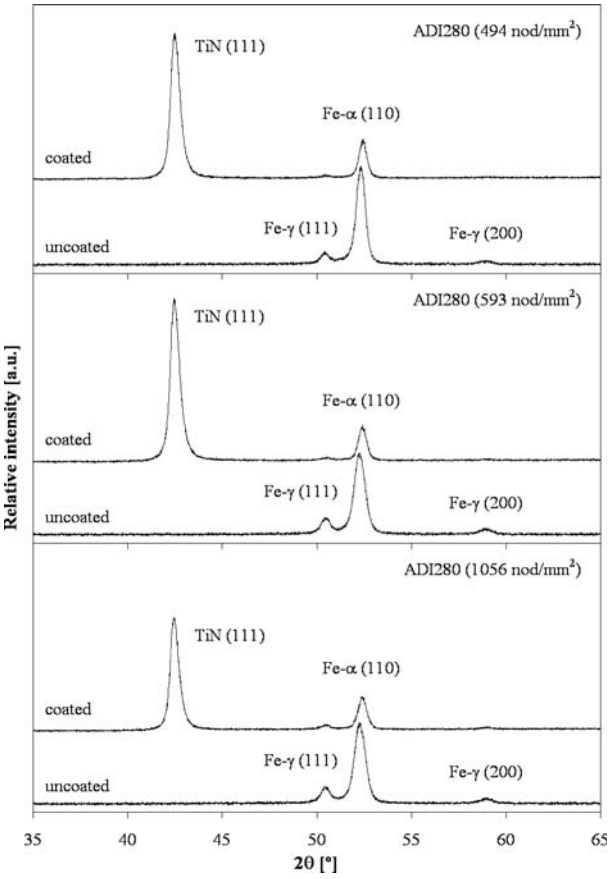

Fig. 1. XRD patterns of ADI280 uncoated and coated samples.

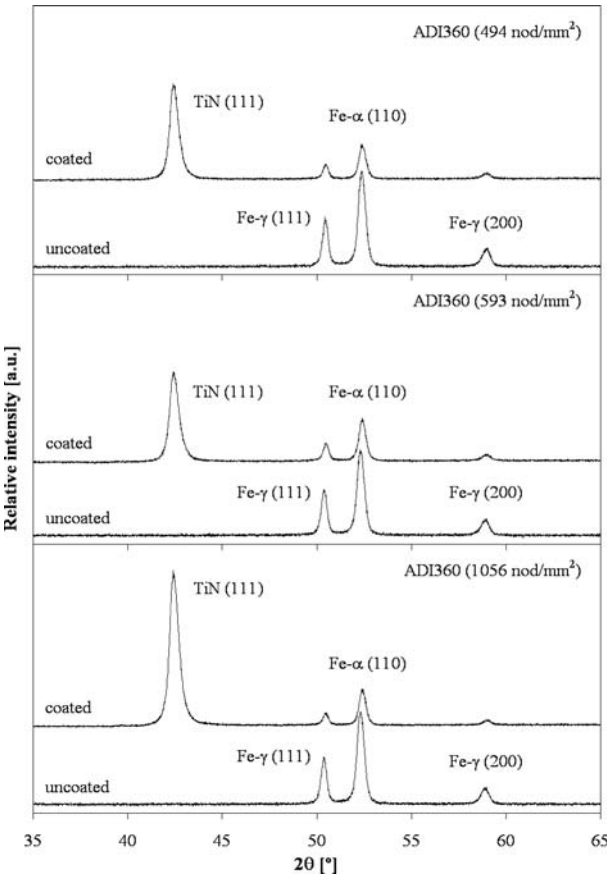

Fig. 2. XRD patterns of ADI360 uncoated and coated samples.

ritic microstructure characteristic of ADI. The patterns of the coated samples do not only reveal the main diffraction peak of TiN, but also some peaks of the phases belonging to the substrates, since the penetration depth of the X-rays is greater than the coatings thickness. On all the substrates, TiN coatings were grown with a preferred orientation of (111) planes parallel to their surface. This strong (111) preferred orientation has been commonly observed for TiN coatings deposited by PVD techniques.[17,18] The change in the relative intensity of the TiN (111) peak in the different samples can be attributed to small variations in film thickness.[19,20] Contaminants presence was not detected within the 2θ range sweeped.

3.2. Substrates Microstructure

Figures 3 and **4** compare the microstructures of ADI substrates before and after coating deposition.

Figures 3(a)–3(c) and 4(a)–4(c) illustrate typical ausferritic microstructures of low and high austempering temperature, respectively. As it can be seen, a lower austempering temperature and a thinner casting thickness promote a higher nodule count and a finer ausferritic microstructure. Figures 3(d)–3(f) and 4(d)–4(f) show that, after coating deposition, ADI's microstructures do not suffer significant changes, at least under the observation conditions employed.

Figure 5 compares volume percentage of retained austenite and Knoop hardness of ADI substrates before and after coating deposition.

After coating deposition, slight differences in the retained austenite content can be observed, while no evidence of hardness decrease is noticed in the different ausferritic microstructures. Therefore, it can be assumed that the deposition parameters utilised in the PVD coating process were not detrimental to ADI's microstructure.

It is worth noting that the increase of the retained austenite content with the rise of austempering temperature is in line with the data reported by other authors.[21,22]

3.3. Surface Topography

Figure 6 compares the arithmetic average roughness (Ra) and surface skewness (Rsk) of the samples before and

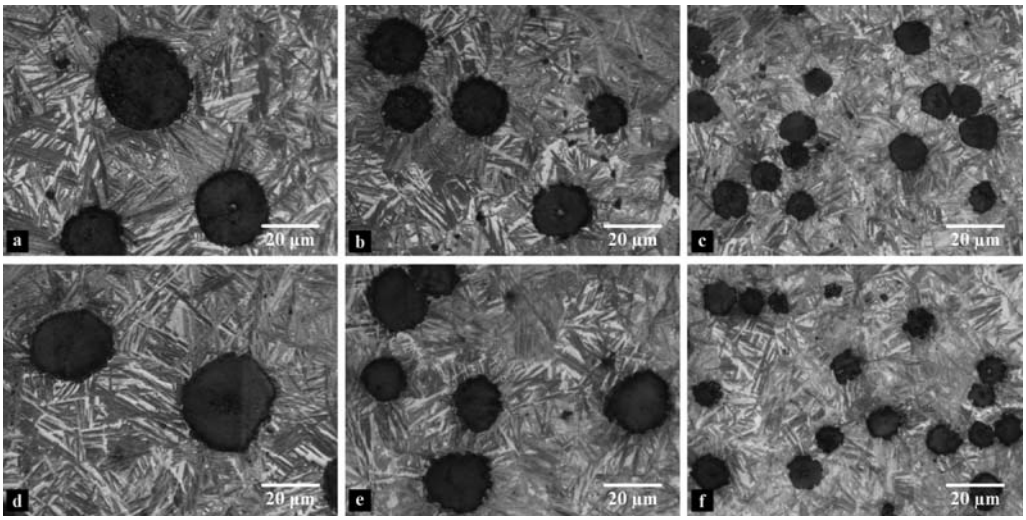

Fig. 3. Microstructure of ADI280 before and after AIP process: (a) ADI 494 nod mm^{-2}, (b) ADI 593 nod mm^{-2}, (c) ADI 1 056 nod mm^{-2}, (d) ADI-TiN 494 nod mm^{-2}, (e) ADI-TiN 593 nod mm^{-2}, (f) ADI-TiN 1 056 nod mm^{-2}.

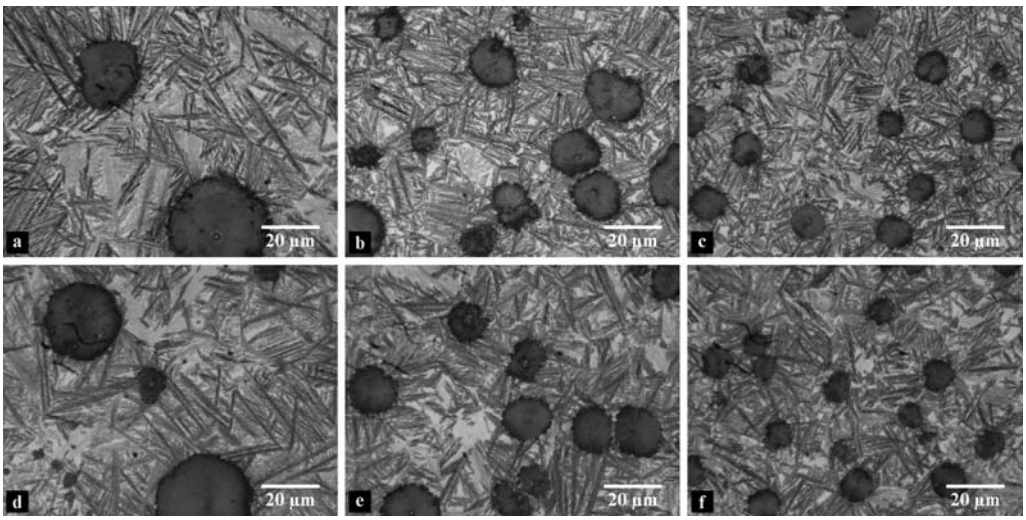

Fig. 4. Microstructure of ADI360 before and after AIP process: (a) ADI 494 nod mm^{-2}, (b) ADI 593 nod mm^{-2}, (c) ADI 1 056 nod mm^{-2}, (d) ADI-TiN 494 nod mm^{-2}, (e) ADI-TiN 593 nod mm^{-2}, (f) ADI-TiN 1 056 nod mm^{-2}.

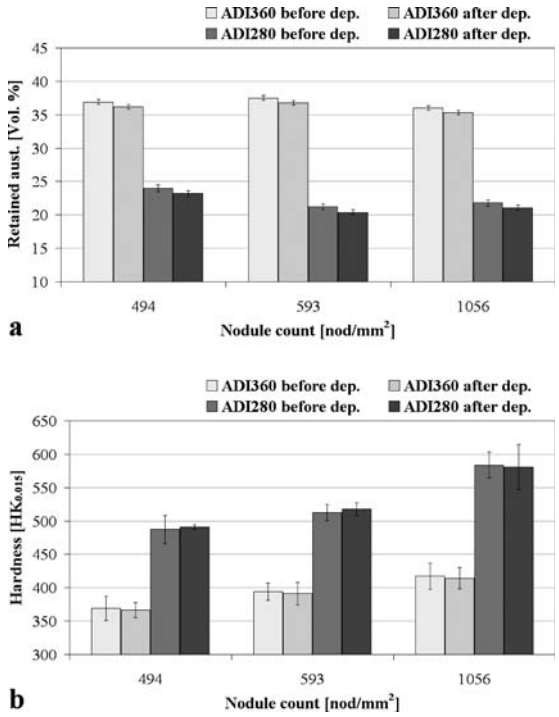

Fig. 5. Comparison of (a) retained austenite content and (b) Knoop hardness of ADI substrates before and after AIP process.

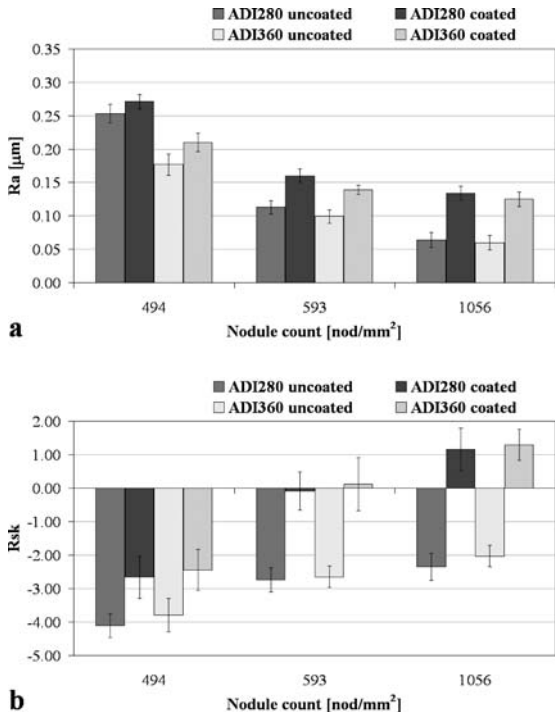

Fig. 6. Roughness parameters of the uncoated and coated samples: (a) arithmetic average roughness, (b) surface skewness.

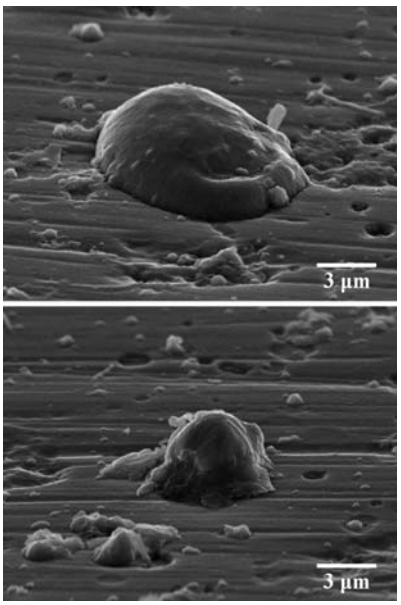

Fig. 7. SEM micrographs showing macroparticles of different sizes attached to the TiN coatings.

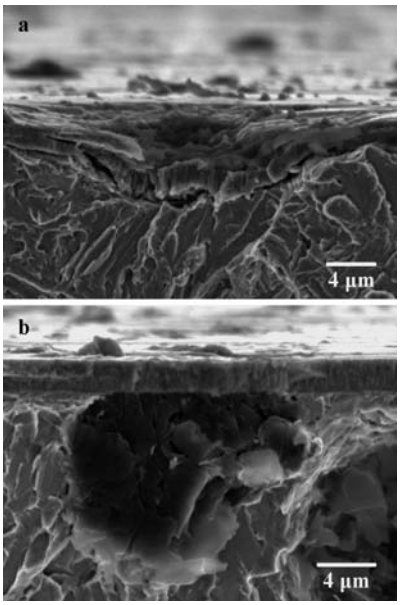

Fig. 8. SEM micrographs showing the effect of surface nodules on the resulting topography of coated samples: (a) craters generated due to graphite removal, (b) film continuity is not altered by the presence of graphite nodules.

after coating deposition.

As it can be noted, the Ra and Rsk parameters of the uncoated samples (substrates) increase as the nodule count decreases for each ADI set analysed. What is more, the presence of craters in their surface predominates (Rsk$<$0). These facts can be ascribed to the coarsening of the matrix structure as nodule count decreases (see Figs. 3 and 4) as well as to the partial or complete graphite removal of certain surface nodules during the specimen preparation stage, whose impact becomes more distinct for larger nodule sizes. Graphite removal from the surface nodules is explained by the polishing method employed (manual polishing with SiC waterproof paper) and by its low mechanical resistance in relation to the metallic matrix.[23)]

In Fig. 6 can also be seen that the Ra and Rsk parameters of the substrates do not vary significantly between the different ADI sets for each nodule count analysed. In general, the ranges of values overlap and only Ra for the lower nodule count shows slight differences between ADI280 and ADI360.

The coating deposition process modifies the surface topography, leading to an increase in Ra and to a change in

Rsk. These alterations can be assigned to a characteristic phenomenon of the cathodic arc PVD process, in which the evaporation of the target material is always accompanied by the release of small amounts of liquid particles (also referred to as macroparticles) incorporated into the plasma as drops, transported towards the substrate surface and attached to the film as metallic Ti, increasing its roughness.[24] The amount of macroparticles present in the coatings and their size distribution, are mainly dependent on the deposition technique and processing parameters utilised.[25–27]

It can be noted that the influence of the coating deposition, due to the presence of macroparticles attached to the film, is greater on the substrates of lower roughness (medium and high nodule counts) in which the Ra variations are greater and surface protrusions become more predominant (Rsk≥0). **Figure 7** depicts the presence of macroparticles on the coatings surface.

Figure 8(a) shows that the film follows the irregularities appearing on the surface of the substrates during the polishing stage. Based on the film aspect on the crater, it could be stated that it acts as a surface defect that promotes an irregular film formation. Furthermore, Fig. 8(b) demonstrates that the continuity of the film is not altered by the presence of surface nodules which bore the polishing stage without being removed.

Therefore, it can be asserted that the resulting topography of the coated samples is dependent on the surface topography of the substrates as well as on the topography induced by the deposition process used. While the former depends on the microstructural characteristics of the substrates and surface preparation method employed, the latter is mainly explained by the attachment to the film of macroparticles of different sizes generated during deposition.

3.4. Coating Characteristics

Table 3 lists the film thickness, hardness and adhesion strength quality values corresponding to each coated sample.

Film thicknesses in the range of 1.7 to 2.0 μm are in agreement with the values reported in the literature,[28] yet the deposition time in this work was longer. Even though most of the processing parameters applied are similar, the use of a large industrial reactor increases the substrate-to-target and substrate-to-chamber wall distances, thereby decreasing the deposition rate.[29,30] This translates into lower film thickness for a given deposition time.

As a way of example, **Fig. 9** shows a fractured cross section used to measure the film thickness of one of the coated samples. As depicted, TiN coatings exhibit a columnar structure with grains perpendicularly oriented to the substrates surface.

Knoop hardness of the coated samples falls within the range of values reported in the literature.[31] **Figure 10** shows that the ranges 1875–2108 HK for ADI280 and 1702–1809 HK for ADI360 follow the hardness trend of their respective substrates. As a consequence, the values derived from this method would be influenced by the substrate characteristics.

The indentation response of a coated sample is contingent on the indenter penetration depth (h) and the coating thickness (t). Values of $h/t>1$ denote that the indenter has severely deformed and penetrated the coating, reaching the underlying substrate material. Therefore, the sample response is dominated by the substrate properties. At the other extreme, values of $h/t<0.1$ indicate that the influence of the substrate on the deformation is small and that the sample response is dominated by the coating characteristics. Values of h/t between 0.1 and 1, in turn, result in a mixed response influenced by the substrate and coating characteristics.[32]

Knoop indentations, on the one hand, were performed using the smallest available load (15 g) that allowed to measure the dimensions of the imprints by using an optical microscopy but, on the other hand, the applied load resulted in h/t ratios between 0.18 and 0.21, *i.e.*, within the range of mixed response.

In order to minimise the influence of ADI substrates on the hardness of the coated samples, instrumented nanoindentation tests were performed by limiting the h/t ratio to values below 0.1 by controlling the applied load. **Table 4** accounts for the hardness and elastic modulus values obtained for each coated sample.

No evidence of substrates influence on the mechanical

Table 3. Film thickness, Knoop hardness and adhesion strength quality of ADI coated samples.

Sample	Nodule count [nod/mm^2]	Film thickness [μm]	Hardness [$HK_{0.015}$]	Adhesion strength quality [HF]
ADI280	494	2.0 ± 0.1	1870 ± 32	1 – 2
	593	1.9 ± 0.2	1951 ± 36	1 – 2
	1056	1.9 ± 0.2	2215 ± 47	1 – 2
ADI360	494	1.8 ± 0.1	1710 ± 36	1 – 2
	593	1.7 ± 0.2	1785 ± 36	1 – 2
	1056	2.0 ± 0.1	1865 ± 49	1 – 2

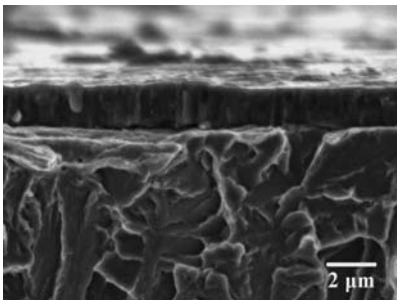

Fig. 9. SEM micrograph showing the thickness and morphology of the TiN coating deposited on ADI280 1 056 nod mm^{-2}.

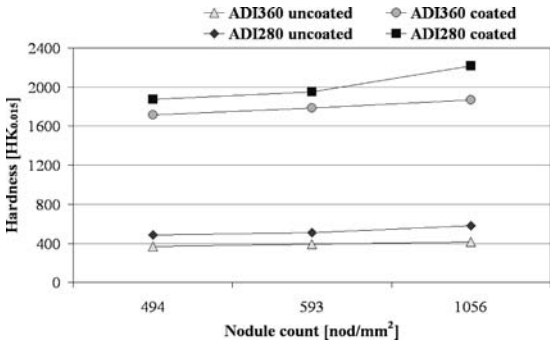

Fig. 10. Comparison of Knoop hardness of the coated and uncoated samples.

Table 4. Hardness and Young's modulus of the coated samples obtained from instrumented nanoindentation tests.

Sample	Nodule count [nod/mm^2]	Hardness [GPa]	Young's modulus [GPa]
ADI280	494	24.63 ± 0.94	326.92 ± 7.53
	593	24.76 ± 0.80	329.53 ± 5.29
	1056	24.22 ± 0.74	323.01 ± 17.04
ADI360	494	24.76 ± 0.75	335.81 ± 2.31
	593	24.70 ± 1.22	326.22 ± 5.76
	1056	24.57 ± 0.75	329.07 ± 4.90

properties of the coated samples was obtained from the instrumented nanoindentation tests. Hardness and Young's modulus values are consistent with those reported by other authors for TiN coatings.[19,33–35)]

The adhesion strength quality of the coating to ADI substrates can be related to indices ranging from HF1 to HF2. No delaminations occurred in any case. It is worth noticing that the hardness differences between substrates as well as nodule count differences with casting thickness variation yielded no effect on coating adhesion. **Figures 11** and **12**

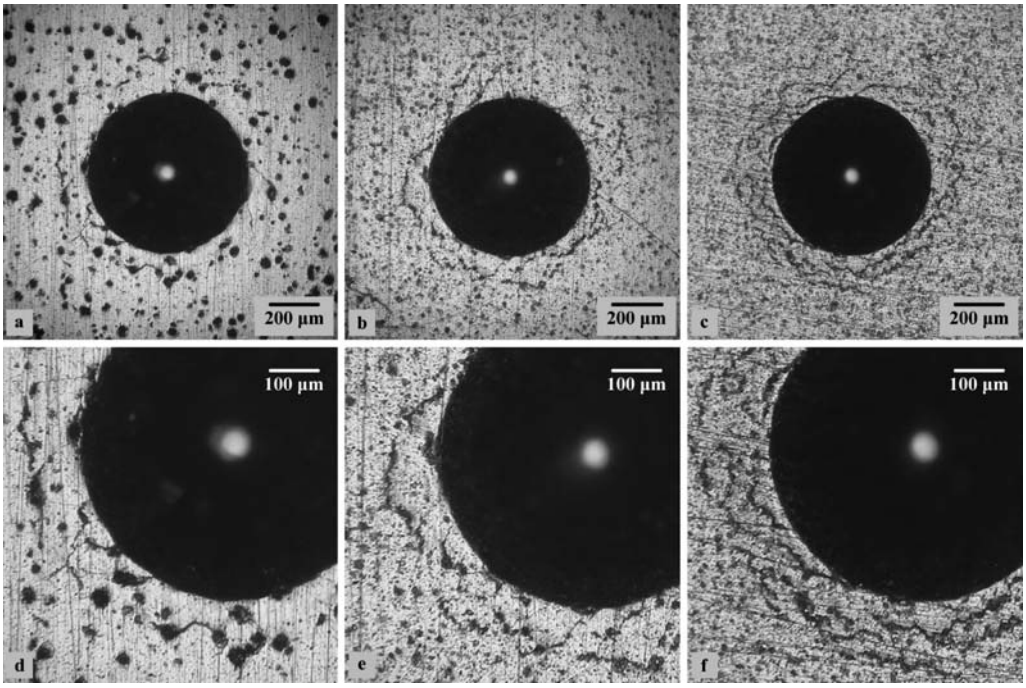

Fig. 11. Cracking patterns of ADI280 coated samples after the Rockwell-C adhesion test: (a) and (d) 494 nod mm^{-2}, (b) and (e) 593 nod mm^{-2}, (c) and (f) 1 056 nod mm^{-2}.

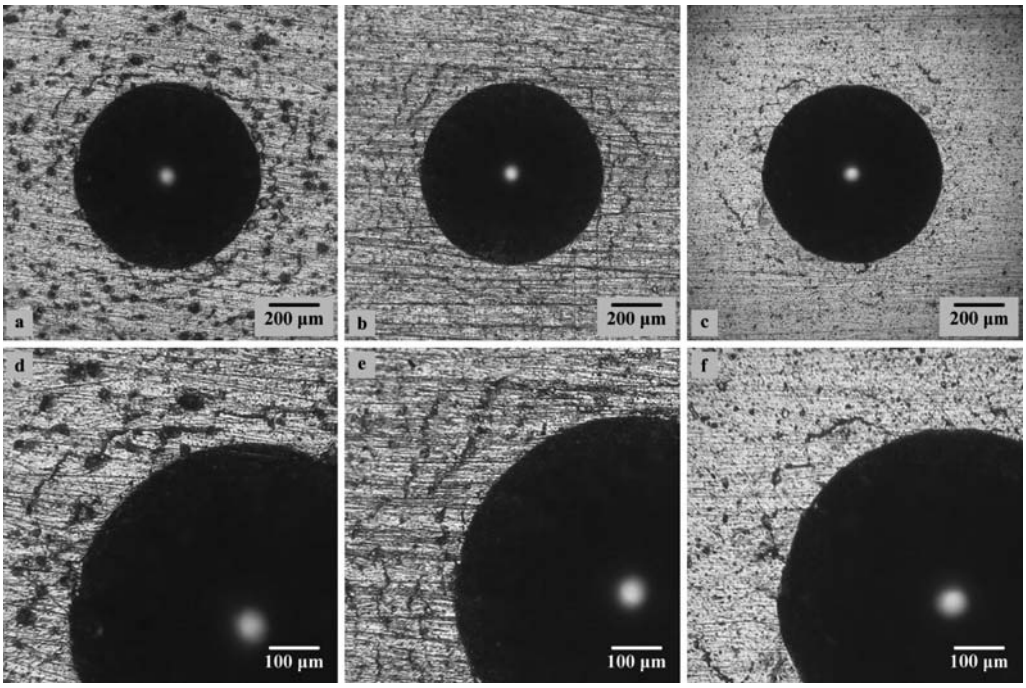

Fig. 12. Cracking patterns of ADI360 coated samples after the Rockwell-C adhesion test: (a) and (d) 494 nod mm^{-2}, (b) and (e) 593 nod mm^{-2}, (c) and (f) 1 056 nod mm^{-2}.

show the imprints resulting from the Rockwell-C adhesion test. Cracking patterns are not entirely in accordance with those tabulated in the standard, yet a preponderance of circumferential cracks exists around the indentations. A first analysis indicates certain influence of the surface nodules present in ADI, since the cracks propagate mainly among the craters originating in the substrates due to the preferential removal of graphite. Further studies should be conducted in order to advance our understanding in the influence that surface nodules exert in the cracking mechanisms of the coatings.

4. Conclusions

TiN coatings deposited on ADI substrates of different nodule count and austempered at 280 and 360°C, were grown with a strong preferred orientation of (111) planes parallel to the surface. All the coatings exhibited the typical columnar structure with grains perpendicularly oriented to the substrate surface.

After the coating process, the ausferritic microstructure of ADI substrates only suffered negligible changes. Moreover, the volume percentage of retained austenite, main parameter to evaluate the substrate degradation, decreased slightly. Substrate hardness reduction after deposition was not detected.

The surface topography of the coated samples is dependent on the microstructural characteristics of the substrates and the surface preparation method employed as well as on the topography induced by the deposition process used. The latter is mainly explained by the attachment to the film of metallic Ti macroparticles of different sizes generated during deposition, wich promotes increases in Ra and changes in Rsk.

Knoop hardness of the coated samples was influenced by the substrates characteristics. The values ranged from 1 875 to 2 108 HK for ADI280 and from 1 702 to 1 809 HK for ADI360, as the nodule count increased from 494 to 1 056 nod mm^{-2}.

The mechanical properties obtained from the instrumented nanoindentation tests were not affected by the substrates. Hardness values were close to 24.6 GPa, while Young's modulus values indicated some scattering (323.01 to 335.81 GPa).

The adhesion strength quality of the coatings can be related to indices between HF1 and HF2. Neither the hardness differences between the different substrates nor the nodule count variation within the range evaluated affected such quality. Cracking patterns were not entirely in agreement with those tabulated in the standard, due to the predominance of circumferential cracks around the indentations.

Acknowledgements

The authors wish to thank the company Sudosilo S.A. for its generous collaboration in coatings deposition.

REFERENCES

1) J. R. Keough: *Eng. Cast. Solut.*, **3** (2001), 42.
2) J. R. Keough, T. Dorn, K. L. Hayrynen, V. Popovski, S. Sumner and A. Rimmer: *Met. Cast. Des. Purch.*, **11** (2009), 28.
3) R. A. Martinez, R. E. Boeri and J. A. Sikora: *Trans. Am. Foundry Soc.*, **106** (1998), 27.
4) C. Labrecque, M. Gagne and G. Liao: Proc. of the 2008 Keith Millis Symp. on Ductile Cast Iron, AFS, Schaumburg, (2008), 64.
5) Ö. N. Dogan, K. K. Schrems and J. A. Hawk: *Trans. Am. Foundry Soc.*, **111** (2003), 949.
6) M. Caldera, J. M. Massone, R. E. Boeri and J. A. Sikora: *ISIJ Int.*, **44** (2004), 731.
7) P. David, J. Massone, R. Boeri and J. Sikora: *ISIJ Int.*, **44** (2004), 1180.
8) J. M. Massone, R. E. Boeri and J. A. Sikora: *Int. J. Cast Met. Res.*, **9** (1996), 79.
9) H. P. Feng, S. C. Lee, C. H. Hsu and J. M. Ho: *Mater. Chem. Phys.*, **59** (1999), 154.
10) C.-H. Hsu, K.-L. Chen and J.-H. Lu: *Surf. Coat. Technol.*, **203** (2008), 868.
11) C.-H. Hsu, J.-K. Lu and R.-J. Tsai: *Mater. Sci. Eng. A*, **398** (2005), 282.
12) D. M. Mattox: ASM Handbook, Vol. 5, Surface Eng., ASM Int., Ohio, (1994), 538.
13) E. S. Gadelmawla, M. M. Koura, T. M. A. Maksoud, I. M. Elewa and H. H. Soliman: *J. Mater. Process. Technol.*, **123** (2002), 133.
14) W. Oliver and G. Pharr: *J. Mater. Res.*, **7** (1992), 1564.
15) H. Ljungcrantz, M. Oden, L. Hultman, J. E. Greene and J. E. Sundgren: *J. Appl. Phys.*, **80** (1996), 6725.
16) W. Heinke, A. Leyland, A. Matthews, G. Berg, C. Friedrich and E. Broszeit: *Thin Solid Films*, **270** (1995), 431.
17) R. Rybiak, S. Fouvry, T. Liskiewicz and B. Wendler: *Surf. Coat. Technol.*, **202** (2008), 1753.
18) S.-Y. Yoon, J.-K. Kim and K. H. Kim: *Surf. Coat. Technol.*, **161** (2002), 237.
19) W.-J. Chou, G.-P. Yu and J.-H. Huang: *Surf. Coat. Technol.*, **140** (2001), 206.
20) W.-J. Chou, G.-P. Yu and J.-H. Huang: *Surf. Coat. Technol.*, **149** (2002), 7.
21) G. Francucci, J. Sikora and R. Dommarco: *Mater. Sci. Eng. A*, **485** (2008), 46.
22) M. A. Yescas, H. K. D. H. Bhadeshia and D. J. MacKay: *Mater. Sci. Eng. A*, **311** (2001), 162.
23) J. M. Radzikowska: *Mater. Charact.*, **54** (2005), 287.
24) J. M. Cairney, S. G. Harris, L. W. Ma, P. R. Munroe and E. D. Doyle: *J. Mater. Sci.*, **39** (2004), 3569.
25) M. Egawa, K. Miura, M. Yokoi and I. Ishigami: *Surf. Coat. Technol.*, **201** (2007), 4873.
26) S. G. Harris, E. D. Doyle, Y. C. Wong, P. R. Munroe, J. M. Cairney and J. M. Long: *Surf. Coat. Technol.*, **183** (2004), 283.
27) T. Matsue, T. Hanabusa and Y. Ikeuchi: *Vacuum*, **74** (2004), 647.
28) C.-H. Hsu, M.-L. Chen and K.-L. Lai: *Mater. Sci. Eng. A*, **421** (2006), 182.
29) J. Lin, B. Mishra, J. J. Moore, W. D. Sproul and J. A. Rees: *Surf. Coat. Technol.*, **201** (2007), 6960.
30) M.-H. Shiao, S.-A. Kao and F.-S. Shieu: *Thin Solid Films*, **375** (2000), 163.
31) J. Takadoum and H. H. Bennani: *Surf. Coat. Technol.*, **96** (1997), 272.
32) A. M. Korsunsky, M. R. McGurk, S. J. Bull and T. F. Page: *Surf. Coat. Technol.*, **99** (1998), 171.
33) G. Abadias, S. Dub and R. Shmegera: *Surf. Coat. Technol.*, **200** (2006), 6538.
34) J. An and Q. Y. Zhang: *Surf. Coat. Technol.*, **200** (2005), 2451.
35) J.-H. Huang, F.-Y. Ouyang and G.-P. Yu: *Surf. Coat. Technol.*, **201** (2007), 7043.